

Development of Highly Photoactive Mixed Metal Oxide (MMO) Based on the Thermal Decomposition of ZnAl-NO₃-LDH

Humaira Asghar ^{1,*}, Valter Maurino ^{1,2}  and Muhammad Ahsan Iqbal ³¹ Department of Chemistry, University of Torino, Via Giuria 7, 10125 Torino, Italy; valter.maurino@unito.it² JointLAB UniTo-ITT Automotive, Via Quarello 15/A, 10135 Torino, Italy³ Departamento de Ingeniería Química y de Materiales, Facultad de Ciencias Químicas, Universidad Complutense de Madrid, 28040 Madrid, Spain; miqbal@ucm.es

* Correspondence: humaira.asghar@unito.it

Abstract: The highly crystalline ZnAl layered double hydroxides (ZnAl-NO₃-LDHs) are utilized for the potential transformation into mixed metal oxides (MMOs) through thermal decomposition and used further for the photodegradation of phenol to assess the influence of calcination on ZnAl-LDHs with enhanced photoactivity. The structure, composition, and morphological evolution of ZnAl-LDHs to ZnO-based MMO nanocomposites, which are composed of ZnO and ZnAl₂O₄, after calcination at different temperatures (400–600 °C), are all thoroughly examined in this work. The final ZnO and ZnAl₂O₄-based nanocomposites showed enhanced photocatalytic activity. The findings demonstrated that calcining ZnAl-LDHs from 400 to 600 °C increased the specific surface area and also enhanced the interlayer spacing of d₀₀₃ while the transformation of LDHs into ZnO/ZnAl₂O₄ nanocomposites through calcining the ZnAl-LDH precursor at 600 °C showed significant photocatalytic properties, leading to complete mineralization of phenol under UV irradiation.

Keywords: ZnAl-NO₃-LDH; mixed metal oxides; photocatalysis; calcination; ZnO; phenol



Citation: Asghar, H.; Maurino, V.; Iqbal, M.A. Development of Highly Photoactive Mixed Metal Oxide (MMO) Based on the Thermal Decomposition of ZnAl-NO₃-LDH. *Eng* **2024**, *5*, 589–599. <https://doi.org/10.3390/eng5020033>

Academic Editor: Lidia Pino

Received: 29 February 2024

Revised: 26 March 2024

Accepted: 9 April 2024

Published: 11 April 2024



Copyright: © 2024 by the authors. Licensee MDPI, Basel, Switzerland. This article is an open access article distributed under the terms and conditions of the Creative Commons Attribution (CC BY) license (<https://creativecommons.org/licenses/by/4.0/>).

1. Introduction

Zinc oxide- and titanium dioxide-based nanomaterials are typical metal oxide nanostructures that are proven to be important for photocatalytic applications [1,2]. However, ZnO and TiO₂ are also broad bandgap metal oxides that can be photoexcited only when exposed to UV light [3]. Although bandgap narrowing can be achieved by increasing the top of the valence band or decreasing the bottom of the conduction band via doping or other methods, there are still unresolved issues, such as substrate mass transfer onto the surface and high rates of photoexcited carrier recombination. Photocatalysts with large pore volume and surface area are necessary for an effective alternative and efficient treatment [3,4]. Recently, mixed metal oxides have been widely reported for their interesting properties that enhance their catalytic activity [5–10]. In contrast to conventional photocatalysts i.e., ZnO or TiO₂, mixed metal oxide (MMO) photocatalysts are being found to efficiently separate photo-induced electron hole pairs with the flexibility to modify the band structure and hence extend the service life of the photocatalyst. Furthermore, high-entropy alloys, composed of five or more cations, provide another potential way to modify the material characteristics of heterogeneous photocatalysts [11,12]. Mixed metallic oxides (MMOs), formed by the thermal decomposition of layered double hydroxides (LDHs), are another potential photocatalytic nanomaterial due to their superior light absorption spectrum and charge separation/transport characteristics.

The layered double hydroxides (LDHs), also known as anionic clays, are composed of positively charged brucite-like layers and exchangeable anions with the chemical formula generally described as $[M^{2+}_{1-x}M^{3+}_x \cdot x(OH)_2]A^{n-}_{x/n} \cdot mH_2O$, where M²⁺ is a divalent metal cation (e.g., Mg²⁺, Zn²⁺, Ni²⁺, Ca²⁺, etc.), M³⁺ is a trivalent cation (e.g., Al³⁺, Fe³⁺, Cr³⁺, etc.), and Aⁿ⁻ is an exchangeable anion such as CO₃²⁻, NO₃¹⁻, SO₄²⁻, etc. Due to the

variation in metal composition, even ternary or quaternary metal composition is possible along with high anionic exchange capacity and anisotropic structure [13–16]. Furthermore, eco-friendly LDHs have a “memory effect” that supports material sustainability, which is required for dye degradation [17–20] and other photocatalytic processes. It is also well-known that LDHs, upon calcination, undergo phase transformation to MMOs through sequential dehydration, dehydroxylation, and elimination of interlayer anions, wherein various layers are stacked one above another in different fashions and thus can obtain different polytypes with random or ordered stacking [21–23]. Numerous studies have been published where the calcined LDH structure was employed to remediate heavy metal contamination and showed better effectiveness than uncalcined LDHs [10,24]. The use of layered double hydroxides (LDHs) as anion immobilization agents requires knowledge of their stability under the operating conditions in which they are intended to be used, which is dependent on the M^{2+}/M^{3+} ratio used for LDH synthesis and must always be considered to propose a strategy for increasing photocatalytic efficiency while keeping the reconstitution mechanism of LDHs in mind for sustainability purposes. As previously stated [25,26], ZnO has been demonstrated to have greater absorption efficiency throughout a broader proportion of the solar spectrum than TiO_2 . The main limitation of ZnO as a photocatalyst is the fast recombination rate of photogenerated electron hole pairs, which disrupts the photodegradation cycle. As a result, significant efforts have been made to enhance ZnO's optical characteristics by reducing band gap energy and limiting the recombination of photogenerated electron hole pairs. Since ZnO nanoparticles were evenly distributed within ZnO-based LDOs, the parent LDH acted as a substrate during the reconstruction process in an aqueous solution, ensuring the sustainability of the system. As a result, the potential class of ZnAl- NO_3 -LDHs can be taken into consideration for potential application to obtain ZnO-based mixed metal oxides. Recently, Suárez-Quezada et al. reported the impact of calcined ZnAl-LDHs into ZnO/ $Zn_6Al_2O_9$ and ZnO/ $ZnAl_2O_4$ heterojunctions by thermal treatment at 400, 500, 600, and 700 °C and utilized for hydrogen production by water splitting reaction [27]. E.M. Seftel et al. described the 93% efficient methyl-orange photo-oxidation by a ZnAl-LDH with the cationic ratio of 5 and calcined at 500 °C [28]. A. Elhalil et al. reported the preparation of ZnO- $ZnAl_2O_4$ mixed phases by calcination of Zn-Al- CO_3 LDH precursors for the degradation performance of caffeine in aqueous solution [29]. Similar work was completed by Zhang et al., where the RhB photodegradation was conducted to conclude the photocatalytic activity of calcined ZnAl-LDHs due to the improved crystal structure and the better separation of photogenerated electron hole pairs [30]. Abdullah Ahmed et al. reported the transformation of ZnAl- NO_3 -LDHs into a ZnO phase and $ZnAl_2O_4$ spinel and found that the crystallinity of the ZnO phase increased with an increase in calcination temperature (600–1000 °C) so as the photodegradation behavior [31]. In summary, the literature describes the effect of the calcination temperature range and metallic cationic ratio (1–5) on photodegradation behavior for liquid and gas phase pollutants.

Although there have been reports of relatively high conversion efficiency in the literature, further research is required to determine the temperature range at which ZnAl-LDHs transform into MMOs without undergoing spinal shape morphology, as this is the difficult part of reconstructing ZnAl-LDHs (>600 °C). The mixed metal oxides formed by the thermal decomposition of LDHs (<600 °C) can be regenerated into the original layered structure when they are in contact with feasible anionic solution. The purpose of this work is to improve our understanding of the activity of calcined ZnAl-LDHs with high crystallinity, which comes from the controlled synthesis of ZnAl- NO_3 -LDHs by adjusting the metallic cationic ratio (M^{2+}/M^{3+}) and by the choice of intercalated anions (NO_3). The highly crystalline ZnAl- NO_3 -LDH (2:1) is reported in this work and was further thermally decomposed up to 400–600 °C to achieve MMOs for potential photocatalytic material. The relationship between the calcined LDH structure and the corresponding photochemical properties was also explored, with particular emphasis on the influence of ZnAl-LDHs calcined at 600 °C on LDH geometry. The calcination temperature is chosen to allow for

the restoration of the LDH structure, making it a sustainable photocatalysis model. The developed MMO layers from ZnAl-LDHs were utilized to optimize the photodegradation of phenol used as a model pollutant, which has not yet been investigated for this class of nanomaterials. Calcinating the ZnAl-LDHs will yield nano-dispersed MMOs because the cations in the LDHs' brucite-like layers are uniformly distributed. The effectiveness of calcination in developing MMOs derived from LDH precursors is carefully examined, providing a reasonable understanding of the utilization of these new classes of photocatalysts.

2. Materials and Methods

2.1. Synthesis of ZnAl-NO₃ LDHs

The LDHs were provided by Smallmatek, Lda (Aveiro, Portugal) and processed according to their manufacturing techniques. To summarize the process, a solution of 0.5 M Zn(NO₃)₂·6H₂O and 0.25 M Al(NO₃)₃·9H₂O was added to a 1.5 M NaNO₃ solution while being stirred at room temperature. Throughout the process, a 2 M NaOH solution was gently added to maintain a consistent pH level of 10 ± 0.5. The production took place in a specialized stainless-steel reactor with automatic control of essential parameters such as pH and temperature, as well as precise chemical addition through peristaltic pumps. The resulting mixture was filtered and dried in an industrial spray drier to ensure uniform and finely sized particles. The synthesized ZnAl-NO₃-LDHs were then calcined at various temperatures (400 °C, 500 °C, and 600 °C) and labelled as LDHs-400 °C, LDH-500 °C, and LDH-600 °C, respectively.

2.2. Characterization

The ZnAl-LDHs' microstructural characteristics and morphology were analyzed using scanning electronic microscopy (JEOL-IT300, JEOL Ltd., Tokyo, Japan) coupled with an EDS detector. Thermogravimetric analysis (TGA) was performed using TA Instruments (TGA Q5000 IR thermobalance (New Castle, DE, USA)) at a heating rate of 10 °C/min up to 1000 °C under airflow of 10 mL/min, while differential scanning calorimetry (DSC) analysis was studied using a Mettler DSC30 calorimeter (Columbus, OH, USA) with 10 mg LDH powder under airflow of 10 mL/min and up to 600 °C. The X-ray diffraction analysis (XRD) was executed using a Rigaku X'Pert High Score diffractometer (Rigaku, Tokyo, Japan) under ambient circumstances using a cobalt K-α ($\lambda = 1.54 \text{ \AA}$) emission source at 10 mA and 30 kV settings. The step size of 0.005° was modified within a 2θ range of 5–70°.

The surface functional groups and chemical bonding of the samples upon calcination were analyzed through attenuated total reflectance-Fourier transform infrared spectroscopy (ATR-FTIR, Thermo Scientific, Waltham, MA, USA) using an Excalibur Series instrument. The measurements were conducted within the range of 550 to 4000 cm⁻¹, with a resolution of 4 cm⁻¹ and 32 scans, employing a diamond crystal as the internal reflective element.

To measure the photocatalytic activity of the catalyst, irradiating suspensions (loading 1 g/L) in the photoreactor with a fluorescent source with $\lambda_{\text{max}} = 365 \text{ nm}$ (Philips PL-S 9W BLB, CO.FO.MEGRA, Milan, Italy, integrated irradiance = 20 W·m⁻²). The photocatalytic activity was calculated as the initial rate of phenol photo-transformation by fitting disappearance curves to an exponential decay. An Oceans Optics spectrophotometer with a cosine-corrected optical fiber probe was used to measure incident radiant power in the 290–400 nm range. The spectrophotometer was spectroradiometrically calibrated using an NIST traceable UV-Vis light source (Micropack DH-2000, THERMO FINNIGAN UV-VIS Plus Detector USA). The starting phenol concentration was 0.1 mM. Measurements were carried out using ultrapure water as a solvent. To evaluate the pollutant adsorption in the material, the reaction mixture was kept in the dark for 0.5 h with magnetic stirring. To assess reaction progress, 0.8 mL aliquots of the irradiation solution were sampled at given time intervals using a syringe with a nylon filter (0.45 μm pore size) to separate the suspended photocatalyst particles. The phenol concentration was determined using an Agilent Technologies HPLC chromatograph 1200 Series (Thermo Finnigan Instrument, Palmer, MA, USA) equipped with a diode array detector, binary gradient high-pressure pump, and an automated sampler. Isocratic elution

was performed using a 20/80 acetonitrile/formic acid aqueous solution (0.05% *w/v*) with a flow rate of 0.5 mL/min and an injection volume of 20 μ L. The column utilized was a Kinetex C18 150-2 (150 mm length, 2 mm I.D., 2.6 μ m core-shell particles; Phenomenex, Torrance, CA, USA). The detection was carried out at 220 nm.

3. Results and Discussion

The diffractograms of ZnAl-LDHs showed the characteristic reflection peaks of (003), (006), (110), (009), (012) (110), and (113), confirming the formation of well-ordered ZnAl-LDHs [32]. Peaks for the ZnO and ZnAl₂O₄ phases can be seen in the XRD patterns of the calcined ZnAl-LDH material. ZnO and ZnAl₂O₄ peaks intensified as the calcination temperature increased from 400 to 600 °C; however, at 600 °C, no characteristic LDH peaks were present, indicating that LDHs had decomposed into MMO.

The cell unit parameter is defined as $a = 2d_{110}$, $c = 3d_{003} = 6d_{006} = 9d_{009}$, and the thermal treatment caused the reduction in the unit cell parameter with the increase in temperature (up to 500 °C), while further increase transformed the LDHs in ZnO-based MMOs. The XRD patterns showed that the LDHs have the characteristic peaks of LDHs during thermal treatment from 400 °C to 500 °C but caused the contraction of basal spacing that can be attributed to the interlayer water loss, decomposition of the NO₃ group, indicated by the lower interlayer thickness of the LDHs [18,20,21]. The interlayer spacing d_{003} and d_{006} gradually decreased with the increase in calcination temperature [22]. Calcination at 400 °C caused partial dehydroxylation of the layers and breakdown of interlayer carbonate anions, while over 500 °C led to the development of ZnO and ZnAl₂O₄ nanoparticles. As the calcination temperature increased, Zn²⁺ ions were freed from the amorphous phase, resulting in crystalline ZnO nanoparticles doped with Al³⁺. The peak reflections at (003) planes of layered double hydroxide were investigated to determine the basal spacing and the “full-width half maximum” for measuring crystallite size (*D*) using the Scherrer equation. Table 1 shows the cell parameters of ZnAl-LDHs as estimated from the XRD pattern. When comparing the XRD pattern of commercial ZnO (Figure 1e) to that of calcined LDHs at 600 °C, the unique peak at scattering angles of 31.64°, 34.85°, 36.65°, 48.1°, 57.12°, 63.2°, and 68.9° corresponded to (100), (002), (101) (102) (110), (103), and (112) crystal planes were present in LDH-600 °C, exhibiting the presence of ZnO peaks (low intensity) along with ZnAl₂O₄ phases.

Table 1. Unit cell parameters of ZnAl-LDHs and calcined ZnAl-LDHs.

Specimen	Lattice Parameter		Interlayer Distance			Crystallite Size, <i>D</i> /nm
	<i>a</i> /nm	<i>c</i> /nm	<i>d</i> ₀₀₃ /nm	<i>d</i> ₀₀₆ /nm	<i>d</i> ₁₁₀ /nm	
ZnAl-LDH	0.356	2.71	0.90	19.77	60.322	3.227
LDH-400 °C	0.355	2.64	0.88	20.01	60.322	3.147
LDH-500 °C	0.355	2.54	0.85	20.12	60.35	3.033

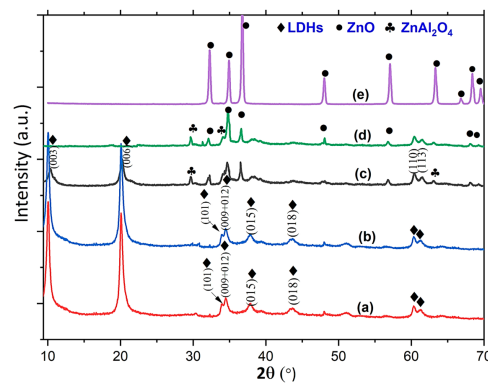


Figure 1. XRD patterns of developed and calcined ZnAl-LDH film samples (a) as-prepared; (b) LDH-400 °C; (c) LDH-500 °C; (d) LDH-600 °C; (e) commercial ZnO.

The developed specimens were further studied using ATR-FTIR in attenuated total reflection mode, as illustrated in Figure 2. The bandwidth exhibited in the region of 3370–3427 cm^{-1} was attributed to the OH^- group stretching, and the absorption band around 1627 to 1633 cm^{-1} due to the flexural oscillation peaks of interlayer water molecules [24]. Moreover, the absorption peaks around 1350 cm^{-1} were assigned to the asymmetric stretching bond of intercalated NO_3^{1-} [27]. The bonds observed at 655 cm^{-1} , 751 cm^{-1} , and 1202 cm^{-1} were associated with the M-OH stretching. The absorption peaks between 550 cm^{-1} and 770 cm^{-1} corresponded to the lattice vibration of metal-oxygen bonds (M-Os) [33]. On calcination, initially, the OH-absorption band receded as the calcination temperature increased. This was followed by a decrease in the NO_3^{1-} absorption peaks, which further indicated the degradation of anionic species inside the LDH galleries. However, at 600 °C, it was found that there were hardly any absorption peaks of anionic species, which induced the structure of LDH transforming to solely include M-OH and M-O groups. This is also well aligned with the commercial ZnO analysis, where the absorption peak of metal-oxygen (ZnO stretching vibrations) vibration mode along with the peaks to the stretching vibration of hydroxyl compounds can be observed [32].

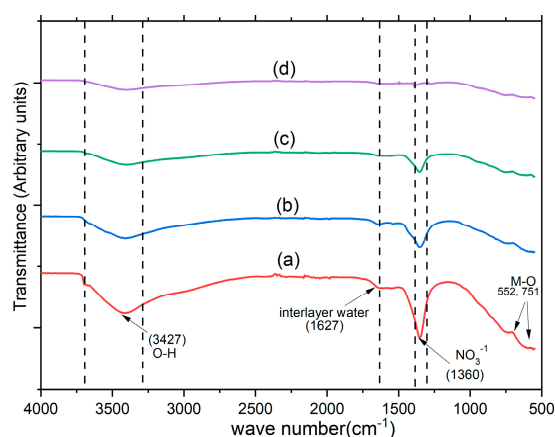


Figure 2. ATR FT-IR spectra of virgin and calcined ZnAl-LDH powder, (a) as-prepared; (b) LDH-400 °C; (c) LDH-500 °C; (d) LDH-600 °C.

Figure 3 demonstrates the generic concept of utilization of MMOs derived from LDHs. The thermal decomposition of ZnAl-LDHs is an indirect construction–reconstruction method in which the mixed oxide obtained after heat treatment of the corresponding LDHs can be brought into contact with a solution containing the anion of interest for re-assembly. During thermal decomposition (Figure 4) the intensity of peaks corresponding to hydroxyl groups decreases, indicating a loss of hydroxyl groups within the LDH interlayers. Additionally, the intensities of peaks related to the NO_3 group also decrease, indicating partial decomposition of the NO_3 group within the interlayer region, particularly within the temperature range up to 400 °C. The TGA-DSC plots highlight the above statements. These findings suggest that the structural decomposition of LDHs occurs in two stages: initially, dehydration of interlayer water molecules occurs around 200 °C, followed by decomposition of interlayer anions and dehydroxylation in a later stage, within the temperature range of 400–600 °C (Figure 4). The obtained findings of this concept are well related to the findings of FT-IR, TGA-DSC, and XRD and with the work provided in previous reports [34–36].

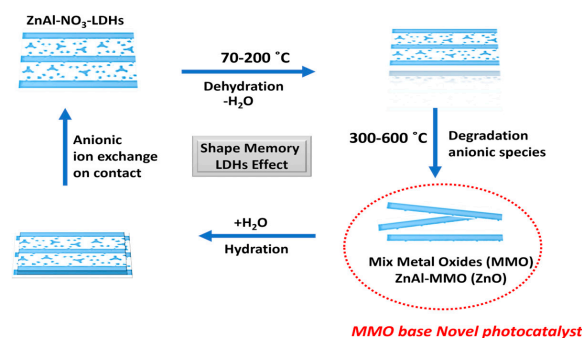


Figure 3. Schematic representation of the memory effect-induced ZnAl-LDH structural transformations.

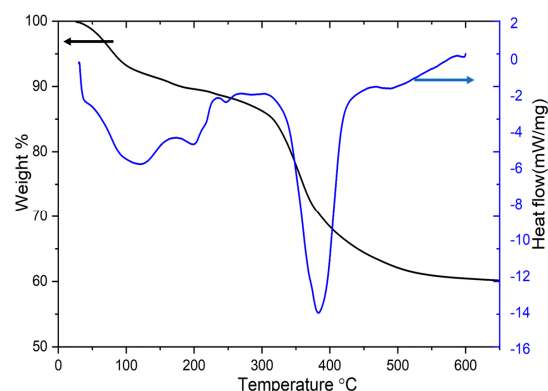


Figure 4. Thermogravimetric analyses of as-prepared ZnAl-NO₃-LDHs.

Scanning electron microscopy (SEM) was used to investigate the microstructure of uncalcined and calcined ZnAl-LDH. Figure 5 shows the different macroscopic morphology at 400 and 600 °C, compared to as-prepared ZnAl-LDHs. It is clear from Figure 5a that initially a well-developed and distinct nano-platelet-shaped ZnAl-LDH structure is formed in which, on decomposition, the nano-sheets of LDH structure are fused to form a spherical flowered structure at 500 °C. ZnO nucleation and guided crystal formation may occur during the breakdown of ZnAl-LDH precursors by increasing the calcination temperature to 600 °C resulting in the directed development of the ZnO and ZnAl₂O₄ phase composition with mixed morphology of distorted nano-belts.

Figure 6 illustrates UV–visible spectra of LDH-600 °C specimen where the spectra show the band gap absorption edges of LDH-600 °C while the large absorption band below 400 nm progressively emerges, indicating that ZnO-based MMO materials can effectively filter UV light [28]. Decomposing the ZnAl-LDH precursor yields a composite material with improved UV-blocking characteristics. The ZnO/ZnAl₂O₄ composite material derived from the ZnAl-LDH precursor has a monodisperse particle size distribution and ZnAl₂O₄ particles are evenly distributed in the network of ZnO nanoparticles due to the direct decomposition of the LDHs. This is due to the high dispersion of the ZnO phase within the amorphous aluminum oxide phase. ZnAl₂O₄ is a versatile material that can function as a catalyst, dielectric, optical material, and transparent conductor. Table 2 displays the computed band gaps of the LDH-600 °C, and the surface area of the ZnO-based MMO material. The band gap of the ZnO/ZnAl₂O₄ MMOs developed by calcination at 600 °C is 2.98 eV, which is smaller than that of pure ZnO and also a second band gap for ZnAl₂O₄ is observed at around 4.25 eV [37].

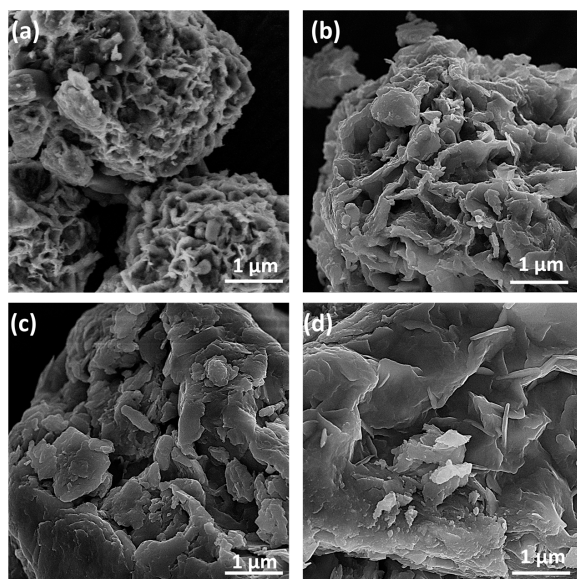


Figure 5. SEM images of uncalcined and calcined ZnAl-LDH films: (a) as-prepared; (b) ZnAl-LDH-400 °C; (c) ZnAl-LDH-500 °C; (d) ZnAl-LDH-600 °C.

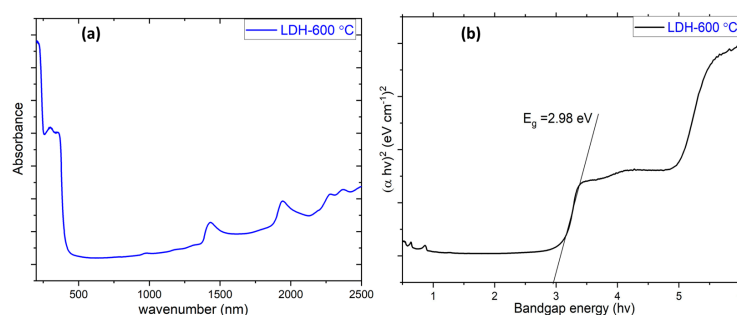


Figure 6. (a) Absorbance spectra; (b) band gap value determined by UV spectroscopy.

Table 2. BET surface and band gap energy value of developed materials.

	Photon Energy (eV)	S _{BET} (m ² g ⁻¹)
ZnAl-LDH	5.3	44.75
LDH-400 °C	4.9	48.09
LDH-500 °C	3.9	51.11
LDH-600 °C	2.98	71.86

This is attributed to the coupling between ZnO and ZnAl₂O₄ in the final composite. ZnO-based MMO materials may be tailored for optical and semiconductor characteristics by adjusting their composition and structure through calcination temperature. The ZnAl (2:1) molar ratio is more systematic for thermal decomposition and the derived MMOs are more economical than other complicated fabrication methods.

The photocatalytic activity of the developed samples was evaluated by monitoring the oxidative photo-transformation of phenol (Figure 7). In the absence of any photocatalysts, about 98% of dye molecules remained after 120 min of UV irradiation. Modelling of the experimental data (phenol concentration as a function of UV/Vis illumination time) was performed using a pseudo-first-order kinetics model (Langmuir–Hinshelwood model) (Equation (1)):

$$\ln(C/C_0) = -kt \quad (1)$$

where C_0 is an initial concentration, C represents the concentration at time t , and k is the reaction rate constant. The decomposition of phenol concentration with time shows first-order kinetics for all the samples. Data in Figure 7 were fitted to an exponential decay and the initial disappearance rates of phenol were calculated and reported in Table 3. From these results, the photodegradation of phenol involves two stages, the first is the degradation of phenol to intermediate products, while the second involves the mineralization of the intermediate compounds to carbon dioxide and water. The hydroxyl groups attached to defects (such as oxygen and surface defects) promote the trapping of photo-induced electron-hole pairs, hence improving their separation [38].

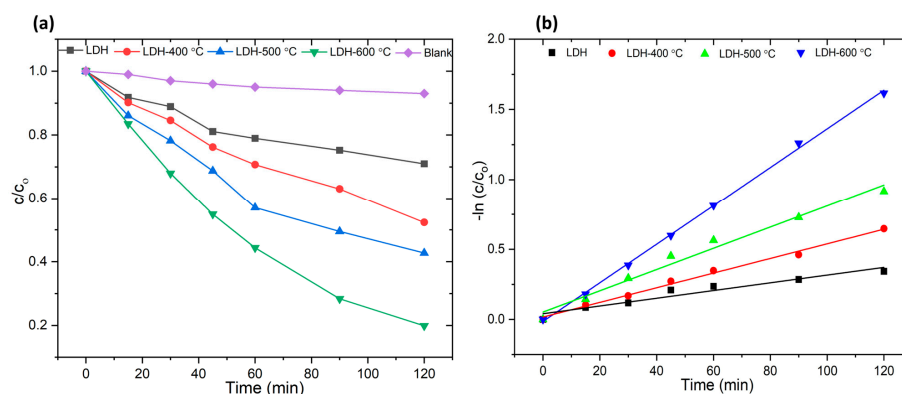


Figure 7. (a) Phenol photodegradation of developed LDHs; (b) pseudo-first order kinetic plots.

Table 3. Constant rate (k) and decomposition rate (χ) of phenol for ZnAl-LDH-based nanomaterials.

Material	Removal Efficiency	Time	K_1 (min^{-1})	R^2	Pseudo-First Order Degradation Rate
	(%)	(min)			($\text{mM} \cdot \text{min}^{-1}$)
ZnAl-LDH	20.19	120	0.0033	0.9694	0.000310
LDH-400 °C	47.63	120	0.0051	0.9939	0.000471
LDH-500 °C	59.17	120	0.0071	0.9951	0.000651
LDH-600 °C	80.12	120	0.0136	0.9995	0.001268

The rate constant of the catalysts increases with increasing calcination temperature, specifically between 400 and 600 °C. This is because the higher calcination temperature generates more active sites and UV light availability, which improves photocatalytic activity. When the calcined materials were assessed for photocatalytic activity under UV light, it was observed that the degradation of phenol after 120 min of irradiation was higher with the material calcined at 600 °C as compared to the material without calcination. The photocatalytic process in this reaction can be explained with the exposure of calcined photocatalyst to UV light photons which cause the electrons (e^-) in the valence band to become excited, causing them to rise to the conduction band. When a photon is absorbed in the conduction band ($e^- \text{CB}$), a positive hole is formed in the valence band ($h^+ \text{VB}$). Excited electrons in the conduction band react with the photocatalyst, producing super radicals [20,21,30].

As the calcination temperature increases from 400 °C to 600 °C, the percentage of phenol abatement also increases from 47% to 82%. The LDH-600 °C catalyst is the most effective since it eliminates 82% of phenol with a normalized degradation rate of 0.001268 ($\text{mM} \cdot \text{min}^{-1}$). This is well correlated with the XRD and TGA measurements where the developed ZnO and ZnAl₂O₄ composites are found to be highly effective for photodegradation. In this context, the coupling of ZnO and ZnAl₂O₄ groups is an attractive option for MMOs which can contribute to the oxidation processes because of their redox potential with a larger oxidizing ability than OH radicals and can be studied further with doping of various nanomaterials for enhanced photodegradation. To pave the road for effective hybrid sustainable photocatalytic LDH-based materials, mixed metal oxides (MMOs) emerge

as a new strategy to fully utilize metal oxides as photocatalysts because they retain their unique pristine properties, while further optimization can be obtained by doping different nanomaterials (for selective pollutants degradation), allowing the intrinsic catalytic activity limit to be exceeded in heterostructure MMOs, resulting in higher efficiency. The photodegradation value in this study is comparable to the values reported in the literature (Table 4) for commercial ZnO and TiO₂ photocatalytic systems in which significant photodegradation of phenol occurs after a particular period of irradiation. However, it is important to note that (a) the irradiation duration in this study was 120 min with the lamp power of 9 W, and (b) the band gap decreasing to 2.98 eV is appreciable in this work compared to other studies. The improvement of photocatalytic capability is ascribed to the synergistic effect of the hybridization of ZnO/ZnAl₂O₄ heterogeneous, which effectively restrains recombination of photo-generated charge carriers and improves the photocatalytic performance and chemical stability of nanohybrid composite since this pure zinc oxide can undergo photo-corrosion under the incidence of continuous light [39–41]. In comparison to existing procedures, the calcination of LDHs, commonly referred to as layered double oxides (LDOs), emerges as a superior approach toward evenly distributed mixed metal oxides which exhibit enhanced photocatalytic performance along with eco-friendly synthesis procedures and a distinctive “memory effect” that can pave the road towards highly efficient smart photocatalytic materials for the remediation of environmental pollutants. This phenomenon has the potential to have a significant impact on practical photocatalytic applications due to its economic feasibility, ease of synthesis, and flexibility to tune the cationic ratio of LDO parent ions.

Table 4. Some works in the literature containing a comparison of the photocatalytic degradation of phenol.

Photocatalyst	C ₀ Phenol	Degradation Rate	Ref.
ZnO commercial, I = 11 W, (λ _{max} = 254 nm)	30 mg/L	84% photodegradation of phenols occurs at 180 min	[41]
ZnO = 0.2 g/L, I = 125 W, (λ _{max} = 270 nm)	25 ppm	95% degradation of phenol occurs in 130 min.	[42]
ZnO ₂ = 2 g/L, I = 125 W λ _{max} = 366 nm)	50 ppm	99% degradation achieved in 360 min.	[43]
TiO ₂ = 0.5 g/L, I = 125 W, (λ _{max} = 270 nm)	30 mg/L	Complete degradation of phenols occurs at 300 min.	[44]
ZnO LDHs, I = 9 W, (λ _{max} = 365 nm)	30 mg/L	83% photodegradation of phenols occurs at 120 min	This Work

4. Conclusions

The calcined ZnAl-LDH structure in this work is found to be highly effective as a photocatalyst, with thermal treatments of ZnAl-LDHs up to 600 °C. This range is feasible given sustainability and recyclability as LDHs can be reconstructed without going to spiral shape morphology. The high crystallinity of synthesized ZnAl-LDHs, due to the feasible M²⁺/M³⁺ ratio (2:1), is found to be significant for the optimum transformation of LDHs to MMOs. The evolution from ZnAl-LDHs to ZnO/ZnAl₂O₄ composite material has a substantial influence on the UV-absorbing and semiconductor properties. Calcination at 500 °C produced a ZnO phase in a nano-platelet-like structure (hydrotalcite + MMO). As the temperature increased from 500 °C to 600 °C, ZnAl₂O₄ nanoparticles developed in the continuous ZnO phase and aggregated between the two phases (ZnO + ZnAl₂O₄). Since pure zinc oxide can undergo photo-corrosion under continuous incidence light, the developed mixed metal oxides based on ZnAl₂O₄ and ZnO (LDH-600 °C) can be a potential substitute where significant photodegradation efficiencies along with reduced photon energy of 2.8 eV (ZnO) is obtained. The developed MMOs can effectively restrain the re-

combination of photo-generated charge carriers, improving the photocatalytic performance and chemical stability of the nanohybrid composite.

Author Contributions: H.A.: conceptualization, formal analysis, methodology, investigation, writing—original draft; M.A.I.: conceptualization, formal analysis, resources, writing and editing; V.M.: conceptualization, formal analysis, methodology, writing—original draft, project administration, funding acquisition. All authors have read and agreed to the published version of the manuscript.

Funding: V. Maurino gratefully acknowledges funding by Regione Piemonte, Italy, through the project ECOBRAKE “Studio e Sviluppo di materiali frenanti ecologici e a bassa emissione di particolato per applicazioni automotive”—L.R. 34/2004—D.D. n° 409 del 02 November 2021. M.A. Iqbal is grateful for the support of the (Marie Skłodowska Curie grant No 847635), the EMULTICOAT European UNA4CAREER project.

Institutional Review Board Statement: Not applicable.

Informed Consent Statement: Not applicable.

Data Availability Statement: Data is contained within the article.

Conflicts of Interest: The authors declare no conflicts of interest.

References

1. Lin, Y.; Hu, H.; Hu, Y.H. Role of ZnO morphology in its reduction and photocatalysis. *Appl. Surf. Sci.* **2020**, *502*, 144202. [[CrossRef](#)]
2. Kitiyanan, A.; Ngamsinlapasathian, S.; Pavasupree, S.; Yoshikawa, S. The preparation and characterization of nanostructured TiO₂–ZrO₂ mixed oxide electrode for efficient dye-sensitized solar cells. *J. Solid State Chem.* **2005**, *178*, 1044–1048. [[CrossRef](#)]
3. Fan, G.; Sun, W.; Wang, H.; Li, F. Visible-light-induced heterostructured Zn–Al–In mixed metal oxide nanocomposite photocatalysts derived from a single precursor. *J. Chem. Eng.* **2011**, *174*, 467–474. [[CrossRef](#)]
4. Zahra, M.; Shariatnia, Z.; Jourshabani, M.; Mahmood, S.; Darvishi, R. ZnO photocatalyst revisited: Effective photocatalytic degradation of emerging contaminants using S-doped ZnO nanoparticles under visible light radiation. *Ind. Eng. Chem. Res.* **2020**, *59*, 15894–15911.
5. Israel, W. Recent conceptual advances in the catalysis science of mixed metal oxide catalytic materials. *Catal. Today* **2005**, *100*, 79–94.
6. Xin, H.; Li, Y.; Wang, H.; Zhang, Q. Controlled preparation of β -Bi₂O₃/Mg–Al mixed metal oxides composites with enhanced visible light photocatalytic performance. *Res. Chem. Intermed.* **2020**, *46*, 5009–5021.
7. Zheng, J.; Li, W.; Tang, R.; Xiong, S.; Gong, D.; Deng, Y.; Zhou, Z.; Li, L.; Su, L.; Yang, L. Ultrafast photodegradation of nitrobenzene by Ag/Ag₃PO₄/Zn–Al LDH composites activated by persulfate system: Removal efficiency, degradation pathway and reaction mechanism. *Chemosphere* **2022**, *292*, 133431. [[CrossRef](#)]
8. Nasser, S.; Sayed, M. Stover ash-extracted mixed oxides surface-doped with Ni for photo-degradation of water organic pollutants. *Int. J. Environ. Anal.* **2023**, *103*, 8941–8956.
9. Zheng, J.; Fan, C.; Li, X.; Yang, Q.; Wang, D.; Duan, A.; Ding, J. Enhanced photodegradation of tetracycline hydrochloride by hexameric AgBr/Zn–Al MMO S-scheme heterojunction photocatalysts: Low metal leaching, degradation mechanism and intermediates. *J. Chem. Eng.* **2022**, *446*, 137371. [[CrossRef](#)]
10. Lorena, G.; Santos, G.; Eguiluz, K.; Salazar-Banda, G.; Lanza, M.; Saez, C.; Rodrigo, M. Towards a higher photostability of ZnO photo-electrocatalysts in the degradation of organics by using MMO substrates. *Chemosphere* **2021**, *271*, 129451.
11. Parisa, E.; Wang, Q.; Razavi-Khosroshahi, H.; Fuji, M.; Ishihara, T.; Edalati, K. Photocatalytic hydrogen evolution on a high-entropy oxide. *J. Mater. Chem.* **2020**, *8*, 3814–3821.
12. Parisa, E.; Shen, X.; Watanabe, M.; Ishihara, T.; Arita, M.; Fuji, M.; Edalati, K. High-entropy oxynitride as a low-bandgap and stable photocatalyst for hydrogen production. *J. Mater. Chem.* **2021**, *9*, 15076–15086.
13. Iqbal, M.A.; Sun, L.; Fedel, M. Synthesis of novel cone-shaped CaAl-LDH directly on aluminum alloy by a facile urea hydrolysis method. *SN Appl. Sci.* **2019**, *1*, 1415. [[CrossRef](#)]
14. Iqbal, M.A.; Asghar, H.; Iqbal, M.A.; Fedel, M. Sorption of As (V) from aqueous solution using in situ growth MgAl–NO₃ layered double hydroxide thin film developed on AA6082. *SN Appl. Sci.* **2019**, *1*, 666. [[CrossRef](#)]
15. Kumar, Y.D.; Uma, S.; Nagarajan, R. Microwave-assisted synthesis of ternary Li–M–Al LDHs (M = Mg, Co, Ni, Cu, Zn, and Cd) and examining their use in phenol oxidation. *Appl. Clay Sci.* **2022**, *228*, 106655.
16. Yi, L.; Yu, T.; Cai, R.; Li, Y.; Yang, W.; Caro, J. One-pot synthesis of NiAl–CO₃ LDH anti-corrosion coatings from CO₂-saturated precursors. *RSC Adv.* **2015**, *5*, 29552.
17. Guanhua, Z.; Zhang, X.; Meng, Y.; Pan, G.; Ni, Z.; Xia, S. Layered double hydroxides-based photocatalysts and visible-light driven photodegradation of organic pollutants: A review. *J. Chem. Eng.* **2020**, *392*, 123684.
18. Abdul, R.; Ali, S.; Asif, M.; In, S.-I. Layered double hydroxide (LDH) based photocatalysts: An outstanding strategy for efficient photocatalytic CO₂ conversion. *Catalysts* **2020**, *10*, 1185. [[CrossRef](#)]

19. Hanane, B.; Da Silva, E.S.; Cherevan, A.S.; Chafik, T.; Faria, J.L.; Eder, D. Layered double hydroxide (LDH)-based materials: A mini-review on strategies to improve the performance for photocatalytic water splitting. *J. Energy Chem.* **2022**, *64*, 406–431.
20. Xuanang, B.; Zhang, S.; Zhao, Y.; Shi, R.; Zhang, T. Layered double hydroxide-based photocatalytic materials toward renewable solar fuels production. *InfoMat* **2021**, *3*, 719–738.
21. Jiménez-López; Leyva-Ramos, R.; Salazar-Rábago, J.; Jacobo-Azuara, A.; Aragón-Piña, A. Adsorption of selenium (iv) oxoanions on calcined layered double hydroxides of Mg-Al-CO₃ from aqueous solution. Effect of calcination and reconstruction of lamellar structure. *Environ. Nanotechnol. Monit. Manag.* **2021**, *16*, 100580. [[CrossRef](#)]
22. Bayu, W.; Kurniawati, P.; Purbaningtias, T.E.; Jauhari, M.H.; Yahya, A.; Tamyiz, M.; Fatimah, I.; Doong, R.-A. Assessing the effect of calcination on adsorption capability of Mg/Al layer double hydroxides (LDHs). *MRX* **2022**, *9*, 035505.
23. Bin, Z.; Wang, Q.; Mo, L.; Jin, F.; Zhu, J.; Tang, M. Synthesis of Mg-Al LDH and its calcined form with natural materials for efficient Cr (VI) removal. *J. Environ. Chem. Eng.* **2022**, *10*, 108605.
24. Iqbal, M.A.; Fedel, M. Ordering and disordering of in situ grown MgAl-layered double hydroxide and its effect on the structural and corrosion resistance properties. *Int. J. Miner. Metall.* **2019**, *26*, 1570. [[CrossRef](#)]
25. Armaković, S.J.; Savanović, M.; Šiljegović, M.; Kisić, M.; Šćepanović, M.; Grujić-Brojčin, M.; Simić, N.; Gavanski, L.; Armaković, S. Self-Cleaning and Charge Transport Properties of Foils Coated with Acrylic Paint Containing TiO₂ Nanoparticles. *Inorganics* **2024**, *12*, 35.
26. Ong, C.B.; Yong Ng, L.; Mohammad, A.W. A review of ZnO nanoparticles as solar photocatalysts: Synthesis, mechanisms and applications. *Renew. Sustain. Energy Rev.* **2018**, *81*, 536–551. [[CrossRef](#)]
27. Suárez-Quezada, M.G.; Romero-Ortiz, J.; Samaniego-Benítez, E.; Suárez, V.; Mantilla, A. H₂ production by the water splitting reaction using photocatalysts derived from calcined ZnAl LDH. *Fuel* **2019**, *240*, 262. [[CrossRef](#)]
28. Seftel, E.M.; Popovici, E.; Mertens, M.; De Witte, K.; Van Tendeloo, G.; Cool, P.; Vansant, E.F. Zn–Al layered double hydroxides: Synthesis, characterization and photocatalytic application. *Microporous Mesoporous Mater.* **2008**, *113*, 296. [[CrossRef](#)]
29. Elhalil, A.; Elmoubarki, R.; Machrouhi, A.; Sadiq, M.; Abdennouri, M.; Qourzal, S.; Barka, N. Photocatalytic degradation of caffeine by ZnO-ZnAl₂O₄ nanoparticles derived from LDH structure. *J. Environ. Chem. Eng.* **2017**, *5*, 3719. [[CrossRef](#)]
30. Zhe, Z.; Hua, Z.; Lang, J.; Song, Y.; Zhang, Q.; Han, Q.; Fan, H.; Gao, M.; Li, X.; Yang, J. Eco-friendly nanostructured Zn–Al layered double hydroxide photocatalysts with enhanced photocatalytic activity. *CrystEngComm* **2019**, *21*, 4607–4619.
31. Ahmed, A.; Abidin Talib, Z.; Mohd, Z.B.H.; Zakaria, A. Improvement of the crystallinity and photocatalytic property of zinc oxide as calcination product of Zn–Al layered double hydroxide. *J. Alloys Compd.* **2012**, *539*, 154. [[CrossRef](#)]
32. Thongam, D.; Gupta, J.; Kumar Sahu, N. Effect of induced defects on the properties of ZnO nanocrystals: Surfactant role and spectroscopic analysis. *SN Appl. Sci.* **2019**, *1*, 1030. [[CrossRef](#)]
33. Prevot, V.; Forano, C.; Besse, J.P.; Abraham, F. Syntheses and thermal and chemical behaviors of tartrate and succinate intercalated Zn₃Al and Zn₂Cr layered double hydroxides. *Inorg. Chem.* **1998**, *37*, 4293. [[CrossRef](#)]
34. Lagnamayee, M.; Parida, K. A review on the recent progress, challenges and perspective of layered double hydroxides as promising photocatalysts. *J. Mater. Chem.* **2016**, *28*, 10744.
35. Ye, H.; Liu, S.; Yu, D.; Zhou, X.; Qin, L.; Lai, C.; Qin, F. Regeneration mechanism, modification strategy, and environment application of layered double hydroxides: Insights based on memory effect. *Chem. Rev.* **2022**, *450*, 214253. [[CrossRef](#)]
36. Jiao, L.; Ding, P.; Zhu, Z.; Du, W.; Xu, X.; Hu, J.; Zhou, Y.; Zeng, H. Engineering self-reconstruction via flexible components in layered double hydroxides for superior-evolving performance. *Small* **2021**, *17*, 2101671.
37. Dixit, H.; Tandon, N.; Cottenier, S.R.; Lamoen, D.; Partoens, B.; Waroquier, M. Electronic structure and band gap of zinc spinel oxides beyond LDA: ZnAl₂O₄, ZnGa₂O₄ and ZnIn₂O₄. *New J. Phys.* **2011**, *13*, 063002. [[CrossRef](#)]
38. Vaiano, V.; Matarangolo, M.; Murcia, J.; Rojas, H.; Navío, J.; Hidalgo, M. Enhanced photocatalytic removal of phenol from aqueous solutions using ZnO modified with Ag. *Appl. Catal. B* **2018**, *225*, 197–206. [[CrossRef](#)]
39. Fu, H.; Xu, T.; Zhu, S.; Zhu, Y. Photocorrosion inhibition and enhancement of photocatalytic activity for ZnO via hybridization with C60. *Environ. Sci. Tech.* **2008**, *42*, 8064–8069. [[CrossRef](#)]
40. Subash, B.; Krishnakumar, B.; Swaminathan, M.; Shanthi, M. Highly efficient, solar active, and reusable photocatalyst: Zr-loaded Ag–ZnO for reactive red 120 dye degradation with synergistic effect and dye-sensitized mechanism. *Langmuir* **2013**, *29*, 939–949. [[CrossRef](#)]
41. Zhang, H.; Zong, R.; Zhu, Y. Photocorrosion inhibition and photoactivity enhancement for zinc oxide via hybridization with monolayer polyaniline. *J. Phys. Chem. C* **2009**, *113*, 4605–4611. [[CrossRef](#)]
42. Shukla, P.R.; Wang, S.; Ming Ang, H.; Tadó, M. Photocatalytic oxidation of phenolic compounds using zinc oxide and sulphate radicals under artificial solar light. *Sep. Purif. Technol.* **2010**, *70*, 338–344. [[CrossRef](#)]
43. Salah, N.H.; Bouhelassaa, M.; Bekkouche, S.; Boultil, A. Study of photocatalytic degradation of phenol. *Desalination* **2004**, *166*, 347–354. [[CrossRef](#)]
44. Hinda, L.; Houas, A.; Herrmann, J.-M. Photocatalytic degradation of polynitrophenols on various commercial suspended or deposited titania catalysts using artificial and solar light. *Int. J. Photoenergy* **2008**, *2008*, 497895.

Disclaimer/Publisher’s Note: The statements, opinions and data contained in all publications are solely those of the individual author(s) and contributor(s) and not of MDPI and/or the editor(s). MDPI and/or the editor(s) disclaim responsibility for any injury to people or property resulting from any ideas, methods, instructions or products referred to in the content.